Active and Passive Elec. Comp., 1998, Vol. 21, pp. 167–181
Reprints available directly from the publisher
Photocopying permitted by license only

OPTIMIZATION OF THE SYNTHESIS PROCEDURE OF $LiMn_2O_4$ ELECTRODES FOR EFFICIENT RECHARGEABLE LITHIUM CELLS: INFLUENCE OF THE CRYSTALLITE SIZE AND SURFACE DEFECTS ON THE ELECTROCHEMICAL PERFORMANCES OF 3 V $Li_{1+x}Mn_2O_4$ AND 4V $Li_{1-x}Mn_2O_4$ ELECTRODES

N. TREUIL[a], A. DESHAYES[b], J. C. FRISON[c], J. C. GRENIER[a], L. RABARDEL[a], E. SELLIER[a], J. PORTIER[a] and G. CAMPET[a,*]

[a] *Institut de Chimie de la Matière Condensée de Bordeaux du CNRS, Château Brivazac, avenue du Dr. A. Schweitzer, 33608 Pessac, France;*
[b] *Centre National d'Etudes des Télécommunications, 38-40 rue du Général-Leclerc, 92131 Issy-les Moulineaux, France;*
[c] *Centre National d'Etudes des Télécommunications, 2 route de Trégastel, BP 40, 22301 Lanion, France*

(Received 19 February 1998; In final form 15 April 1998)

Various $LiMn_2O_4$ electrode materials, having different crystallite sizes ranging from ~ 50Å to ~ 500Å, have been investigated either in 3V or in 4V Li batteries. In agreement with our ≪electrochemical model≫, we have shown that nanocrystalline samples have much higher capacity and cyclability than their microcrystalline homologue in the 3 V domain uniquely. A reverse trend is observed in the 4 V range, still in agreement with the model.

Keywords: Electrochemical model; Li batteries; nanocrystalline materials

*Corresponding author. e-mail: campet@icmcb.u-bordeaux.fr.

INTRODUCTION

It has been evidenced that lithium manganese oxides having the spinel structure are promising cathodes for lithium batteries because they are cheaper and less toxic than other candidates (cobalt and nickel oxides). It must be recalled that the early spinel materials possessed a satisfactory theoretical specific capacity [1]. However, the practical capacity declined on cycling and only later optimization yielded satisfactory results [2–4]. Synthesis of $LiMn_2O_4$ is often undertaken using solid-state reactions [2–8]. In this procedure, a Mn compound such as MnO_2 (chemically or electrolytically prepared γ-MnO_2, for instance), or Mn_2O_3, or $MnCO_3$, is mixed with a Li compound such as Li_2CO_3, LiOH or $LiNO_3$. The stoichiometric mixture (Li/Mn = 1 in molar ratio) is then calcined between 450°C and 950°C in air or/and argon. In some cases, portions of the $LiMn_2O_4$ product are mixed with a desired amount of Li salt in order to improve the cycling performances [2, 3]. Solution methods have also been advantageously developed [9, 10]. They achieve, indeed, finely-grained homogeneous starting materials and, therefore, lead to ultrafine crystallites of the spinel phase. $LiMn_2O_4$ can also be similarly prepared using polymeric routes. One of them deals with the Pechini process which involves polymeric precursors [11]. We have recently patented another original polymeric route which is adapted to large scale production; the controlled explosive oxidation of the polymer precursors, which occurs at low temperature, leads also to very finely-grained homogeneous starting materials [12].

Our objective, here, is to prepare $LiMn_2O_4$ with controlled crystallite size. Ten years ago, we have indeed shown, using many examples [13], that the control of crystallite size was a key factor determining the specific capacity and the cycling efficiency of the electrodes. We established, for instance, that the electrochemical activity, with regard to lithium, of the polycrystalline films $\ll Li_{0.5}Ni_{0.5}{}^{III}O \gg$ increased as the crystallite size diminished [14]. When the latter was lower than 30Å the corresponding nanocrystalline films reversibly inserted nearly one lithium per nickel; the films had thereby a composition close to $\ll LiNi_{0.5}{}^{II}O \gg$ in their inserted state [14–17]. The importance of such nanocrystalline materials for electrochemical systems, such as electrochromic windows or microgenerators working with Li^+ ions, was quoted [14–17]. We have shown also that the strong electrochemical

activity of $\ll Li_{0.5+x}Ni_{0.5-x}{}^{III}Ni_x{}^{II}O \gg$ was not an individual case: actually, an extended family of nanocrystalline materials was proposed (Li_xSnO_2, Li_xTiO_2, $Li_xFe_2O_3$, *etc.*) having an enhanced electrochemical activity compared with that of their microcrystalline homologue [18–23].

An important ≪electrochemical model≫ was deduced : ≪**Nanocrystalline materials** will have an **enhanced electrochemical activity**, compared with that of their microcrystalline homologue, only if the **first electrochemical process** which intervenes corresponds to a discharge of the Li battery. This discharge will begin with an **electrochemical grafting** of the Li^+ ions at/near the crystallite surface. The structural defects or distorsions at/near the crystallites, which are more obvious in the nanoscale region than in the microscale one, act indeed as reversible grafting sites for Li^+ ions . The following second electrochemical step occurs during the discharge of the Li battery (when the crystallite structure is adapted) : intercalation of the Li^+ ions into the crystallites.

Consequently, the reversible cycling behavior of these efficient nanocrystalline electrode materials can be depicted as : grafting → intercalation → deintercalation → degrafting *etc.* [18, 23].

On the other hand, for another well known family of intercalation materials, such as $Li_{1-x}MO_2$(M = Co, Ni) cycling between the starting composition $LiMO_2$ and between $Li_{1-x}MO_2(x > 0)$, a reverse situation occurs : the insertion and deinsertion ratio of lithium is generally lower in nanosized electrode materials than in microsized ones. The electrochemical cycling of the corresponding electrode materials does not start, here, by a grafting process of the lithium ions because it begins by the removal (*i.e.*, deintercalation) of the Li^+ ions from the electrode; this process will be inhibited by the ungrafted surface defects. Consequently, for this second family of materials, the density of the surface defects which will, therefore, inhibit the deintercalation processes, must be minimized.≫

These concepts are important because they allow us to predict when it is preferable to synthetize nanocrystalline (or microcrystalline) electrode materials for Li batteries, depending upon the first electrochemical process is a discharge (or a charge).

Our objective which is obviously related to these concepts is, as pointed above, to investigate various $LiMn_2O_4$ electrodes having

different crystallite sizes. In this prospect, a solution method has been used : it advantageously involves a synthetic procedure carried out in air [10], unlike other sol-gel methods [9]. We have also successfully used the above mentioned polymeric route [12], but the corresponding study has been reported elsewhere for sake of clarity [22].

EXPERIMENTAL

In order to assess the effect of crystallite size upon the electrochemical behavior of stoichiometric $LiMn_2O_4$ in both the 3 V and 4 V domains, homogeneous starting materials have been heated in air for 20 hr. at different temperatures ranging from 250°C to 800°C. The homogeneous starting materials have been obtained from an aqueous solution of manganese(II) acetate tetrahydrate (Aldrich 99 + %), which was added to an appropriate aqueous solution of lithium carbonate (Aldrich 99,997%). A precipitate is formed at basic pH. The remaining water is removed by rotary evaporation at 70°C and, finally, the finely-grained homogeneous starting materials were obtained after intimate mixing in an agate mortar. The latter were, then, fired in air in order to get phase pure $LiMn_2O_4$ spinels. Weight losses and the corresponding endo or exothermic processes were observed from thermogravimetric (TGA) and differential thermal analysis (DTA).

The average crystallite sizes of the differently grained $LiMn_2O_4$ powders have been deduced from X-ray diffraction analysis and transmission electron microscopy (TEM) using a JEOL JSM-840 apparatus. Surface morphologies were examined using scanning electron microscopy (SEM). The specific surface areas of the products were examined with a single-point Brunauer, Emmett, and Teller (BET) method. The cationic and anionic stoichiometries were controlled using Auger spectroscopy, atomic absorption spectroscopy and electrochemical analysis.

The electrochemical measurements were performed using computer-controlled potentiostat/galvanostat (Tacussel, PGS 201 T model) for the electrochemical cells based on ≪Li // liquid electrolyte // composite cathode≫. The Li anode is a lithium metal foil (Aldrich 99,9%). The liquid electrolyte consists of 1M $LiPF_6$(Aldrich 99,99%)

dissolved in ethylene carbonate (EC, Prolabo 99%) + dimethylcarbonate (DMC, Aldrich 99%) (50/50 by volume). The composite cathodes were prepared by mixing the lithium manganese oxide together with Chevron carbon black and a binder, usually PTFE (*i.e.*, Teflon), in the weight ratios 80:13:7. The mixture is, then, pressed at 1 ton/cm^2 for 1 min. The entire assembly was finally dried under primary vacuum for 15 hr. at 120°C.

All manipulations of air-sensitive materials as well as the cell assemblies were carried out in the inert atmosphere of an argon filled glove box.

RESULTS AND DISCUSSION

Preparation Conditions of $LiMn_2O_4$

For application considerations it is important to determine the lowest temperature at which $LiMn_2O_4$ can be synthesized. In order to do so, we first investigated the role of the starting materials on the synthesis of $LiMn_2O_4$ by means of TGA and DTA analysis (Fig.1). The starting materials are heated in air at a rate of 3°C/mn from 20°C to 600°C. A small exothermic peak centered at 177, 8°C appears, followed by an endothermic peak centered at 224.9°C and which accounts for the fusion of the acetate groups [9]. This melting precedes the very exothermic decomposition of the acetate groups which accounts for the abrupt loss ($\sim$47% weight loss) which is observed in the TGA curve (Fig.1). The lowest temperature at which the phase pure spinel is formed is, obviously, above 225°C (fusion of the acetate groups). It is, indeed, 250°C when the starting materials are heated in air for 20 hr. This temperature corresponds, in fact, to the onset of the exothermic decomposition of the acetate groups (Fig.1), leading to their departure.

The annealing temperature of the starting materials obviously affects the morphology and crystallinity of the resulting $LiMn_2O_4$ and, therefore, will influence the electrochemical properties of the corresponding electrode materials as we have quoted above.Consequently, the precipitates have been separately fired in air for 20 hr. not only at 250°C, but also at 500, 700 and 800°C. Above 800°C, it is

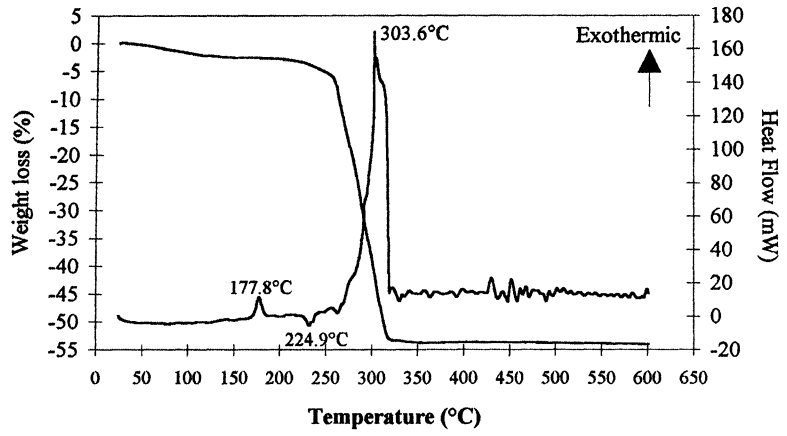

FIGURE 1 DTA/TGA traces of the starting material at 3°C/mn under air atmosphere.

known, indeed, that oxygen deficient materials occur, their anionic deficiency being responsible for their poor cycling efficiency in the 4 V domain [1]. We have illustrated on Figure 2 the oxygen departure above 800°C.

The symbolization of the samples, that we have considered here, is reported in Table I.

Structure and Texture

To determine the structure of each sample, X-ray diffraction (XRD) experiments were carried out. According to them, each sample has the characteristic signature of a spinel (Fig.3). The XRD patterns could be indexed with the same spinel space group as the standard $LiMn_2O_4$ spinel (Fd3m). Let us simply recall that the structure can be described as layers of close packed oxygen, in which lithium and manganese ions occupy tetrahedral (8a sites) and octahedral sites (16d sites) respectively.

As expected, the peaks gradually sharpen with increasing firing temperature due to the increase of the crystallinity. The growth of crystallite sizes is also illustrated on the TEM micrographs (Fig.4): the average crystallite size increases from ~ 50Å for $LiMn_2O_4(250)$ to ~ 1000Å for $LiMn_2O_4(800)$. The specific surface area (deduced from

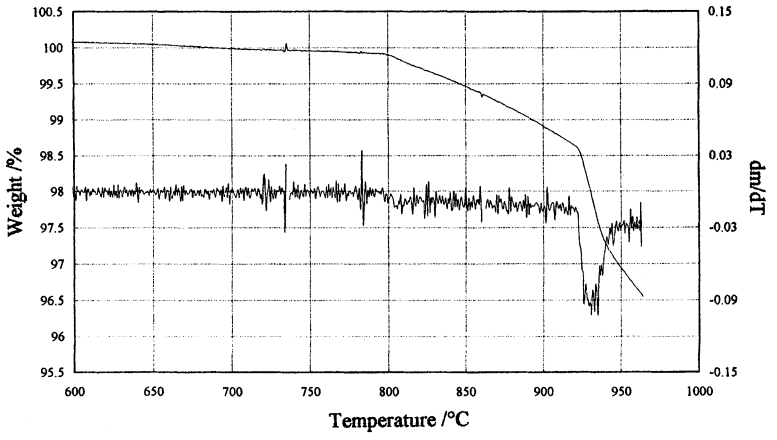

FIGURE 2 TGA trace of the spinel phase (heating rate = 2°C/mn in air atmosphere).

TABLE I Sample symbolization

Firing temperature (°C)	*Sample symbolization*
250	$LiMn_2O_4$(250)
500	$LiMn_2O_4$(500)
700	$LiMn_2O_4$(700)
800	$LiMn_2O_4$(800)

BET analysis) progressively diminishes, as the firing temperature increases, from $\sim 30\,m^2/g$ for $LiMn_2O_4$(250) to $\sim 6\,m^2/g$ for $LiMn_2O_4$(800). These rather low values result from grain agglomerations which are illustrated on Figure 5, showing SEM micrographs. However, we have shown for other electrode materials, and using many examples, that it is not the grain agglomeration but mainly the crystallite size which influences the electrochemical performances of the electrodes [13–23].

Study of the ≪Li // Liquid Electrolyte : $LiPF_6$ + EC + DMC // $LiMn_2O_4$≫ Cells≫: Influence of the Crystallite Size of $LiMn_2O_4$ Powders

The $LiMn_2O_4$ powders fired at different temperatures (Tab. I) were studied for their (de)insertion properties, at constant charge–

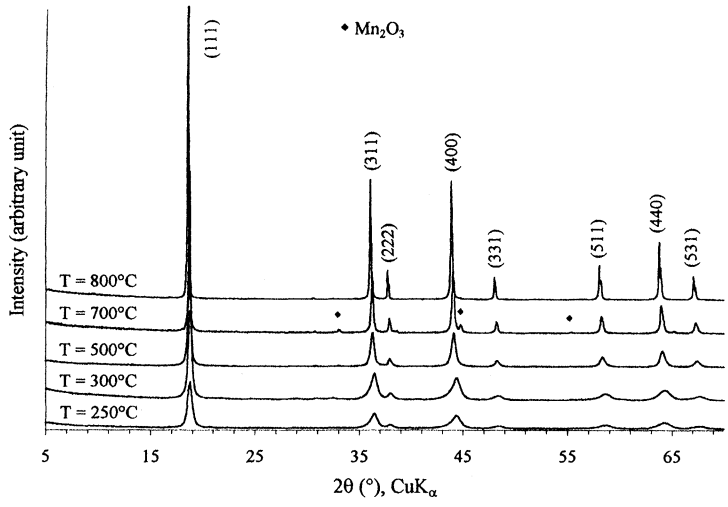

FIGURE 3 X-ray diffraction patterns of the synthesized spinels (Kα, Cu = 1.54 Å).

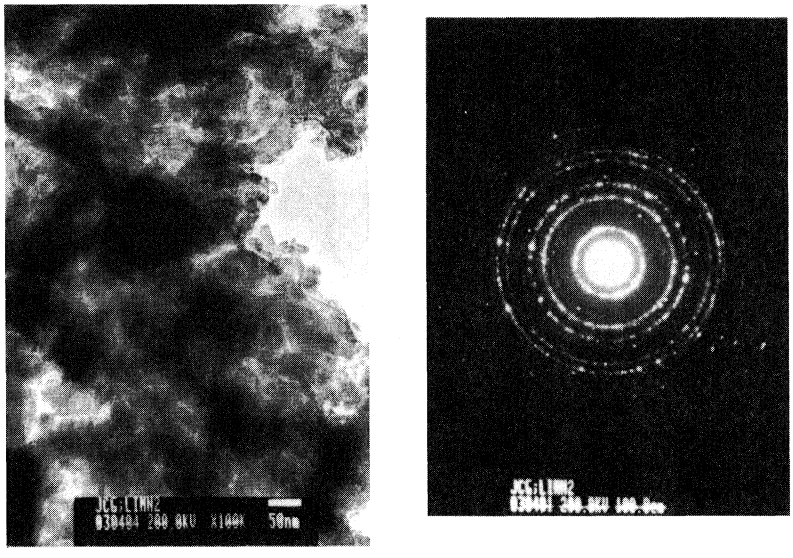

(a)

FIGURE 4 (a): TEM micrograph and Electron Diffraction image of $LiMn_2O_4$(250). (b) and (c) : TEM micrographs of $LiMn_2O_4$(700) and $LiMn_2O_4$ (800).

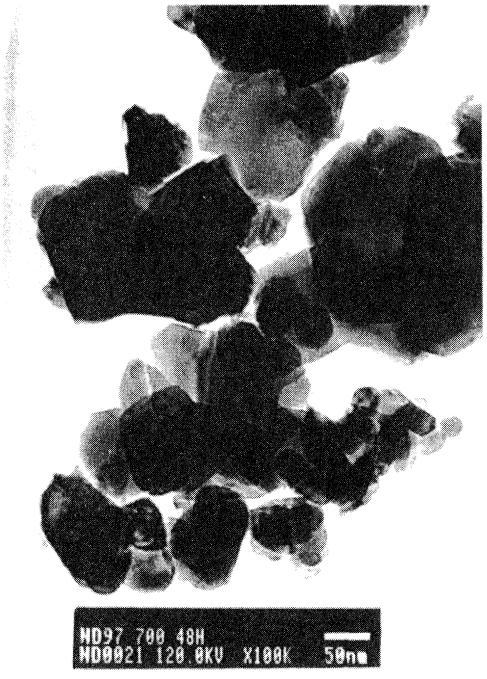

(b)

FIGURE 4 (Continued).

discharge current, over the potential ranges 3.5 – 2.2 V and 4.4 – 3.5 V for 3 V $Li_{1+x}Mn_2O_4$ and 4 V Li_{1-x} Mn_2O_4 respectively.

(a) Constant Current Charge-discharge Behavior of 3V $Li_{1+x}Mn_2O_4$ Cathodes

The cycling data are illustrated on Figure 6. Note that the highest capacity is observed for $LiMn_2O_4$ (250): it is ~two times higher than that of $LiMn_2O_4$(700 or 800). These results are in full agreement with our above mentioned ≪electrochemical model≫: the electrochemical cycling begins, indeed, with a discharge of the cell. Therefore, according to the model the nanocrystalline electrode material must

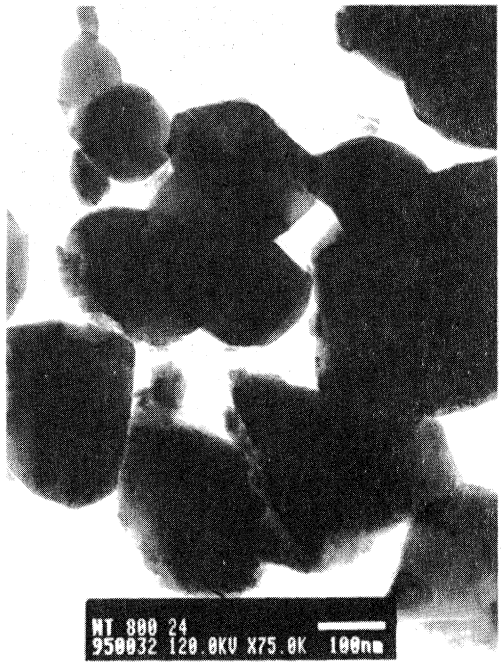

(c)

FIGURE 4 (Continued).

have the highest capacity: it is indeed the case. The repeated cycling behavior of the $LiMn_2O_4$ (250) electrode is excellent (more than 100 cycles at the present time [22]).

(b) Constant Current Charge-discharge Behavior of 4V $Li_{1-x}Mn_2O_4$ Cathodes

In contrast, and as shown on Figure 7, a reverse trend is observed when the cells are cycled within the 3.5–4.4 V voltage domain. The cells using $LiMn_2O_4$(250) have, indeed, a lower capacity than those using $LiMn_2O_4$ (700 or 800): the capacities correspond to $\sim$0.60 mole

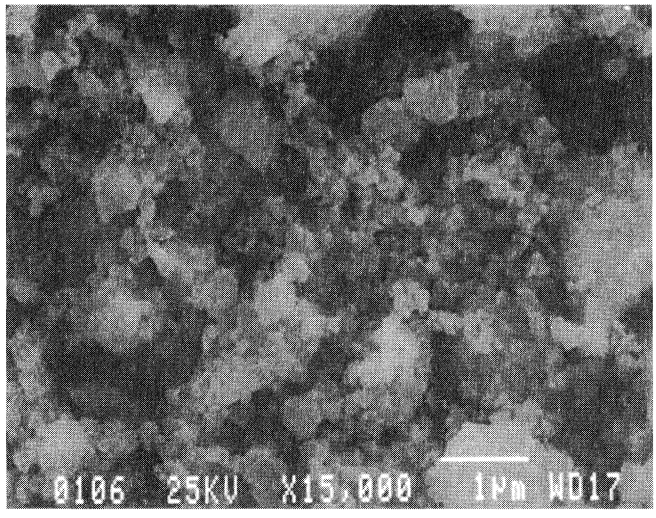

(a)

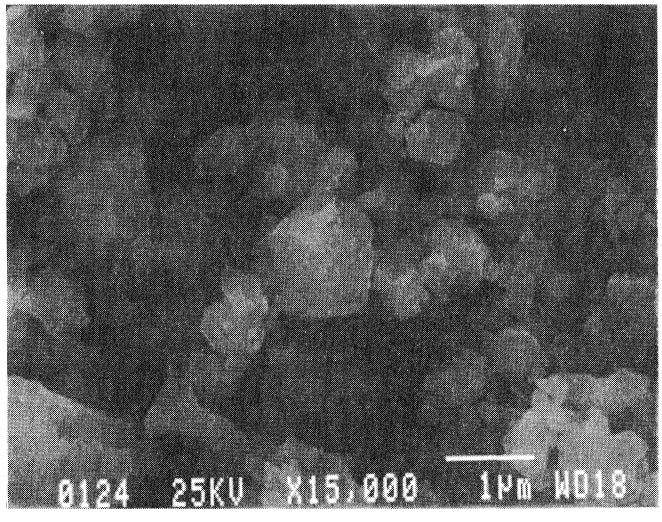

(b)

FIGURE 5 (a) SEM micrographs of : (a) $LiMn_2O_4(250)$; (b) $LiMn_2O_4$ (800).

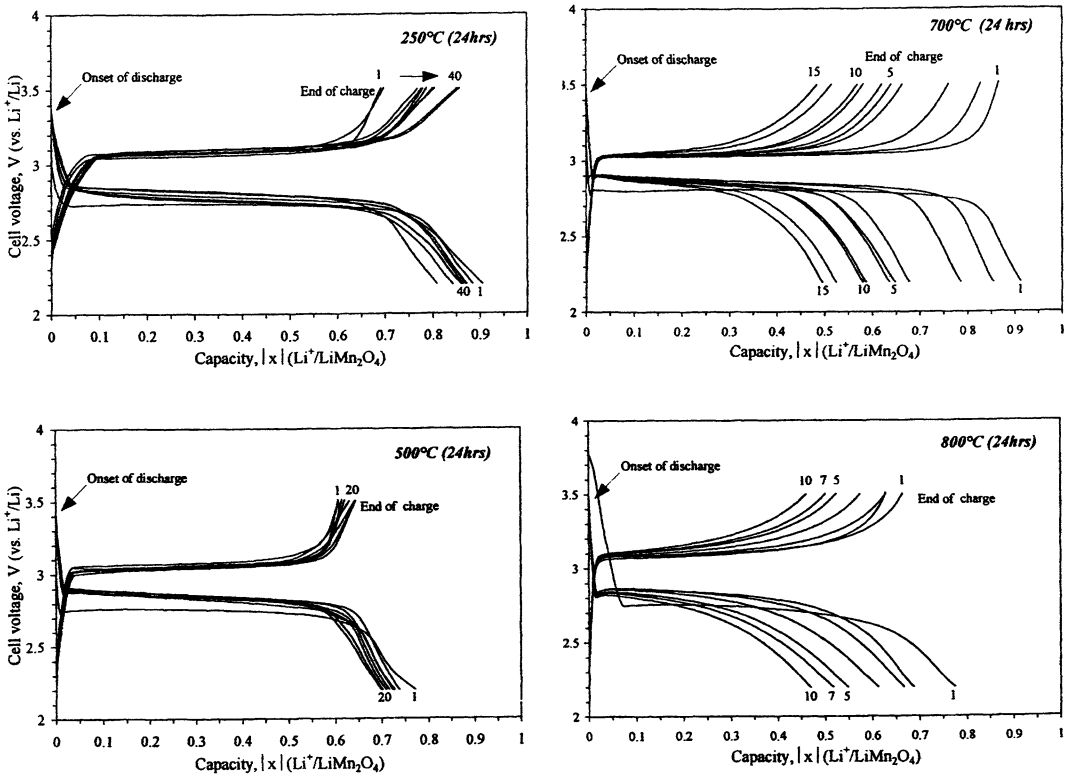

FIGURE 6 Galvanostatic discharge–charge curves at 500 μA in Li//EC-DMC, 1M $LiPF_6$//3V$LiMn_2O_4$ cells, at 25°C (cathode active mass = 20 mg, effective area = 1.33 cm^2).

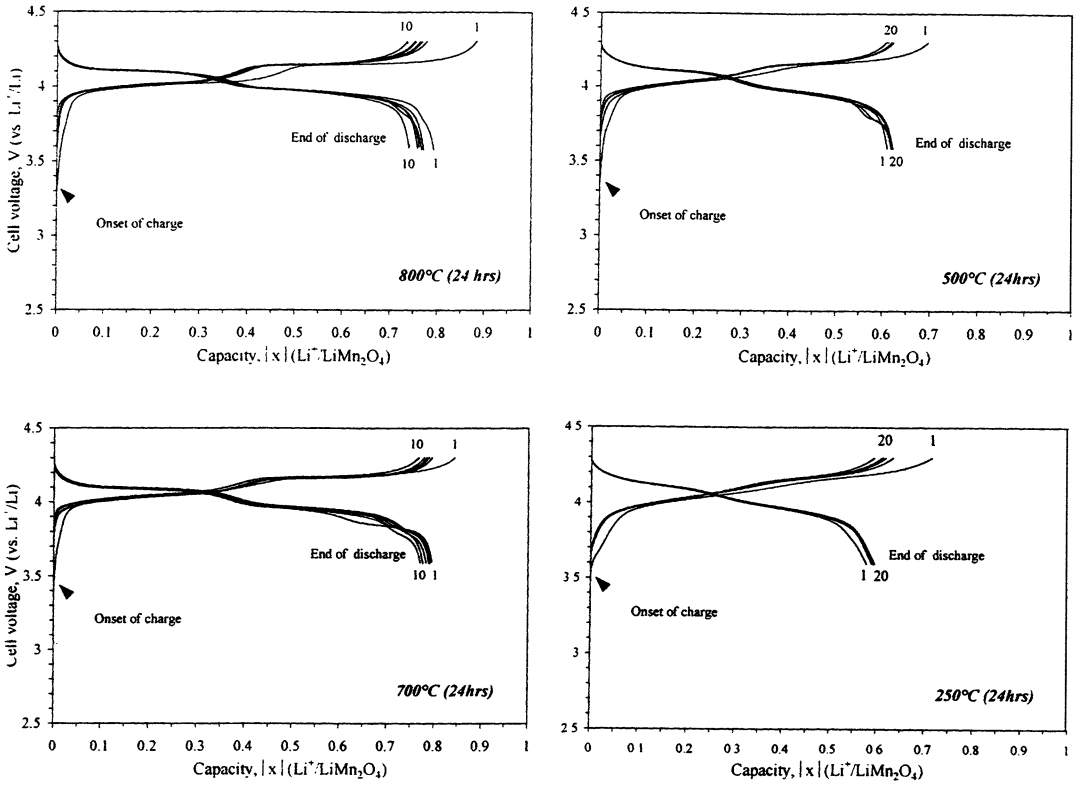

FIGURE 7 Galvanostatic discharge-charge curves at 500 μA in Li//EC-DMC, 1M $LiPF_6$//4V$LiMn_2O_4$ cells, at 25°C (cathode active mass = 20 mg, effective area = 1.33 cm^2).

of Li per mole of $LiMn_2O_4$ for $LiMn_2O_4$(250) and to ~ 0.8 mole of Li per mole of $LiMn_2O_4$ for $LiMn_2O_4$ (700 or 800).

We found that there is nearly no capacity fading for the $LiMn_2O_4$(700 or 800) electrodes under repeated cycling process (more than one hundred cycles at the present time [22]). That gives evidence of the good electrochemical stability of these electrodes. Their cycling curves show two well defined plateaus (Fig.7). We believe that these two plateaus account for a two step extraction process for lithium ions : the Li^+ are first removed, at the time of the first plateau, from half the tetrahedral sites in which Li–Li interactions occur [24]; the other half of the remaining lithium are removed (second plateau) from the other tetrahedral sites in which the Li^+ do not have any nearest neighbor Li–Li interactions [24].

CONCLUSION

Using 3 V $LiMn_2O_4$ and 4 V $LiMn_2O_4$ as non limiting but illustrative examples, we have shown, here, that our ≪electrochemical model≫ can be efficiently used to predict when it is preferable to use: (i) either nanocrystalline electrode materials, such as $LiMn_2O_4$(250) aimed for 3 V Li batteries, having therefore structural defects or distorsions at/near the crystallite surfaces; (ii) or well crystallized electrode materials, such as $LiMn_2O_4$ (700 or 800) aimed for 4 V Li batteries, which are nearly free of structural defects.

In order to get more insight into the relation between the electrochemical properties and structure of such nanosized electrode materials, Mn K-edge XAS study, XPS and Li NMR analysis are being carried out at the present time [25].

Acknowledgements

N. Treuil, G. Campet and J. Portier wish to thank the CNET (≪Centre National d'Etudes des Télécommunications≫-92 Issy les Moulineaux - France) for its helpful assistance and financial support.

References

[1] Hunter, J. C. (1981). *J. Solid State Chem.*, **39**, 142. Thackeray, M. M., David, W. I. F., Bruce, P. G. and Goodenough, J. B. (1983). *Mater. Res. Bull.*, **18**, 461. Goodenough, J. B., Thackeray, M. M., David, W. I. F. and Bruce, P. G. (1984). Revue de Chimie Minérale, **21**, 435.

[2] Gummow, R. J., de Kock, A. and Thackeray, M. M. (1994). *Solid State Ionics*, **69**, 59.

[3] Tarascon, J. M. (1995). US Patent 5, **424**, 205.

[4] Kokband, R. and Barker, J. (1996). *Solid State Ionics*, **84**, 1.

[5] Ohzuku, T., Kitawaga, M. and Hirai, T. (1990). *J. Electrochem. Soc.*, **137**, 769.

[6] Tarascon, J. M., Wang, E., Shokoohi, F. K., McKinnon, W. R. and Colson, S. (1991). *J. Electrochem. Soc.*, **138**, 2859.

[7] Manev, V., Momchilov, A., Nassalevska, A. and Sato, A. (1995). *J. Power Sources*, **54**, 323 and références therein.

[8] Jiang, Z. and Abraham, K. M. (1996). *J. Electrochem. Soc.*, **143**, 1591.

[9] Barboux, P., Tarascon, J. M. and Shokoohi, F. K. (1991). *J. Solid State Chem.*, **94**, 185.

[10] Huang, H. and Bruce, P. G. (1994). *J. Electrochem. Soc.*, **141**, L106.

[11] Liu, W., Farrington, G. C., Chaput, F. and Dunn, B. (1996). *J. Electrochem. Soc.*, **143**, 879.

[12] Treuil, N., Portier, J., Campet, G., Ledran, J. and Frison, J. C. (1998). French patent ; European patent number 97402433.3-2111.

[13] Couput, J. P., Campet, G., Chabagno, J. M., Bourrel, M., Muller, D., Garrié, R., Delmas, C., Morel, B., Portier, J. and Salardenne, J. (1989). *Int. Appl. Publ. Under PCT. Int. Pat. Class GO2F 1701*, F01 G9/00, C 23C 14/34, WO 91/01510.

[14] Geoffroy, C., *Ph. D. Thesis*, Univ. Bordeaux-1, France (1990); see also Morel, B. *Ph. D. Thesis*, Univ. Bordeaux-1, France (1991).

[15] Campet, G., Portier, J. and Morel, B. (1992). Active and Passive Electronic Components, **14**, 219.

[16] Campet, G., Morel, B. and Geoffroy, C. (1991). *Mat. Science and Engineering*, **B8**, 303.

[17] Giron, J. C. (1994). *Ph. D. Thesis*, Univ. Paris-VI, France.

[18] Campet, G. (1996). *Proceedings of the 4th CMC International Symposium on Nanopore*, Nanoparticle and Nanocomposite Chemistry, Sep. 13–14, Seoul Natinal Univ., pp. 72–99.

[19] Han, S. D., Huang, S. Y. and Campet, G. (1991). Active and Passive Electronic Components, **18**, 61.

[20] Huang, S. Y., Campet, G., Treuil, N., Portier, J. and Chhor, K. (1996). Active and Passive Electronic Components, **19**, 189.

[21] Park, N. G., Campet, G., Portier, J. and Choy, J. H. (1998). Active and Passive Electronic Components, to be published.

[22] Treuil, N. (1997). *Ph. D. Thesis*, Univ. Bordeaux-1, France.

[23] Campet, G., Wen, S. J., Han, S. D., Shastry, M. C. R., Portier, J. and Salardenne, J. (1993). *Mat. Science and Engineering*, **B18**, 201.

[24] Xia, Y. and Yoshio, M. (1996). *J. Electrochem. Soc.*, **143**, 825.

[25] Treuil, N., Campet, G., Choy, J. H., Portier, J., Deshayes, A. and Frison, J. C., *J. of Material Chemistry*, (in preparation).